Available online at www.sciencedirect.com
SCIENCE DIRECT®
C. R. Physique 7 (2006) 116–127
COMPTES RENDUS PHYSIQUE
http://france.elsevier.com/direct/COMREN/

Superconductivity and magnetism/Supraconductivité et magnétisme

Superconductivity and macroscopic quantum effects in superconducting/ferromagnetic hybrid nanostructures

Marco Aprili [a,b,*], Takis Kontos [a,1], Maria-Luisa Della Rocca [a,b], Jérome Lesueur [b], Wiebke Guichard [c], Philippe Gandit [c], A. Bauer [d], Christoph Strunk [d]

[a] *CSNSM-CNRS, bâtiment 108, université Paris-Sud, 91400 Orsay, France*
[b] *Laboratoire de physique quantique ESPCI, 10, rue Vauquelin, 75005 Paris, France*
[c] *CRTBT-CNRS, 25, avenue des Martyrs, 38000 Grenoble, France*
[d] *Institut für Experimentelle und Angewandte Physik, Universität Regensburg, 93040 Regensburg, Germany*

Abstract

Hybrid nanostructures not only open new routes for studying the coexistence of superconductivity and ferromagnetism, but they also provide new insights into the fundamentals of quantum electronics. We have investigated, by a series of experiments, the change in the superconducting wavefunction resulting from the interaction between the spins of a Cooper pair and the exchange field. Tunneling spectroscopy reveals an inhomogeneous Fulde–Ferrell–Larkin–Ovchinnikov (FFLO) superconducting state induced in a ferromagnetic thin film by the proximity effect. As a consequence, critical current and macroscopic quantum interference (SQUID) experiments show π-coupling between two superconductors coupled through a ferromagnetic thin film. π-coupling originates a spontaneous half quantum flux in a superconducting ring. This phase transition has been observed by Josephson and Hall magnetometry. ***To cite this article: M. Aprili et al., C. R. Physique 7 (2006).***
© 2006 Académie des sciences. Published by Elsevier SAS. All rights reserved.

Résumé

Supraconductivité et effets quantiques macroscopiques dans les nanostructures hybrides supraconducteur/ferromagnétique. Les nanostructures hybrides ouvrent des nouvelles perspectives pour étudier la coexistence entre deux états fondamentaux antagonistes : la supraconductivité et le ferromagnétisme. Elles permettent également de créer des nouveaux dispositifs pour l'électronique quantique. Nous avons étudié par une série d'expériences l'état supraconducteur original qui se produit à l'intérieur d'un matériau ferromagnétique à cause de l'interaction entre les spins d'une paire de Cooper et le champ d'exchange. Les mesures de spectroscopie tunnel montrent qu'un état supraconducteur inhomogène, de type Fulde–Ferrell–Larkin–Ovchinnikov (FFLO), est induit dans une couche mince ferromagnétique par effet de proximité. Nous avons montré par ailleurs que le couplage Josephson entre cet état et une électrode supraconductrice est négatif (couplage-π) par des mesures de courant critique et d'interférence quantique macroscopique (SQUID). Le couplage π représente une « batterie de phase » et produit un supercourant spontané lorsque la jonction ferromagnétique est insérée dans un anneau supraconducteur. Le flux magnétique associé à ce courant est d'un demi-quantum de flux. Cette transition de phase à basse température a été observée par magnétométrie Josephson et magnétométrie Hall. ***Pour citer cet article : M. Aprili et al., C. R. Physique 7 (2006).***
© 2006 Académie des sciences. Published by Elsevier SAS. All rights reserved.

* Corresponding author.
E-mail address: aprili@lps.u-psud.fr (M. Aprili).
[1] Permanent address: Laboratoire Pierre Aigrain, École normale supérieure, 24, rue Lhomond, 75231 Paris cedex 05.

1631-0705/$ – see front matter © 2006 Académie des sciences. Published by Elsevier SAS. All rights reserved.
doi:10.1016/j.crhy.2006.01.001

Keywords: Superconductivity; Josephson effect; Tunneling spectroscopy; Quantum transport

Mots-clés : Supraconductivité ; Effet Josephson ; Spectroscopie tunnel ; Transport quantique

1. Introduction

Ferromagnetic order breaks time-reversal symmetry. It is therefore detrimental to conventional superconductivity which relies on the pairing of time-reversed states. The Clogston criterion [1] sets the maximum energy that completely destroys the superconductivity. For a three dimensional system $E_{\text{Clogston}} = \Delta_{\text{s}}/2^{1/2}$, where Δ_{s} is the superconducting gap. In fact, as the exchange energy becomes greater than the superconducting gap, corresponding to the bounding energy of a Cooper pair, two electrons in a pair obtain enough energy to align their spins and destroy the pair. Fulde and Ferrell [2], and Larkin and Ovchinnikov [3] have shown independently that a new superconducting state, the so-called FFLO state, can be realized in a ferromagnetic superconductor. For $E_{\text{ex}} \approx E_{\text{Clogston}}$, the superconducting ground state consists of pairs with non-zero center of mass momentum, directly proportional to E_{ex}. Two main difficulties make the FFLO state particularly hard to be observed in bulk materials:

(i) as in the FFLO state, the superconducting gap oscillates in real space (we will address the origin of these oscillations later), in the dirty limit (when the mean free path is smaller than the superconducting coherence length, i.e., $l < \xi_{\text{o}}$), collisions mix electron wave vectors at the Fermi level and the superconducting gap is zero;
(ii) since the exchange field of a ferromagnet is typically much greater (100 meV – 1 eV) than the gap energy ($\Delta_{\text{s}} \approx$ meV), the exchange energy can be replaced by the Zeeman energy (Pauli limit) in a non-magnetic material. In this case, the FFLO state occupies a small part of the magnetic field-temperature phase diagram, around $H_{\text{c}} = E_{\text{Clogston}}/\mu_{\text{B}}$.

These constraints are fundamental and are related to the coexistence of pairing with a ferromagnetic ground state. We overcome this obstacle by spatially decoupling superconductivity and ferromagnetism.

This paper is organized as follows. In Section 2, we describe the superconducting proximity effect in a ferromagnet and the spectroscopic evidence for an induced FFLO state. Then, in Section 3, we show that proximity effect tunneling spectroscopy can directly address the exchange enhanced spin fluctuations and the exchange energy at the ferromagnetic- paramagnetic transition. In Sections 4 and 5 there the critical current and macroscopic quantum interference experiments, respectively, are reported, showing Josephson π-coupling for thickness of the ferromagnetic layer corresponding to a negative induced pair wave function in the ferromagnet. Finally, in Section 6, we show that a π-junction is a 'phase-battery' and can generate spontaneous supercurrents when introduced in a superconducting ring.

2. Superconductor/ferromagnet proximity effect

If we consider a superconductor (S) in direct contact with a ferromagnet (F), Cooper pairs can penetrate into the ferromagnet (F) realizing a state equivalent to FFLO. Since the total energy is conserved, a Cooper pair gains finite momentum $\Delta p = E_{\text{ex}}/\hbar v_F$ in F [4]. In fact, because of the exchange field, the spin up electron must increase its kinetic energy while the spin down electron has to reduce it by the same amount. A center of mass momentum translates into wave function phase variation $\Delta\phi = \Delta p^* x$ as function of distance, x, from the S/F interface. As a result, the pair wave function in the singlet state (up*down-down*up) becomes:

$$\Psi_F = \Psi_{\text{o}}\left(\mathrm{e}^{\mathrm{i}(\phi+\Delta\phi)}\right) + \Psi_{\text{o}}\left(\mathrm{e}^{\mathrm{i}(\phi-\Delta\phi)}\right) \tag{1}$$

and consequently the superconducting order parameter oscillates in real space. We shall call this new superconducting state, induced in the ferromagnet, a π-state to emphasize that a sign change in the pair wave function correspond to a π shift in the superconducting phase. This nomenclature is borrowed from that used for the symmetry of the wave function of unconventional superconductors (i.e., d-wave, p-wave, ...).

If the transport in the ferromagnet is diffusive, the pair function becomes [4]:

$$\Psi_F = f_+ + f_- \sim \cos(x/\xi_F)\mathrm{e}^{-x/\xi_F} \tag{2}$$

where

$$f_{\pm} = \int_0^{\infty} 1/(\pi Dt)^{1/2} \mathrm{e}^{-x^2/2Dt} \mathrm{e}^{\pm 2\mathrm{i}E_{\mathrm{ex}}t}\, \mathrm{d}t$$

The superconducting state is evanescent in F since singlet correlations are destroyed by the exchange field as a result of the non-ergodic dephasing of the electrons of opposite spin forming the Cooper pairs in the diffusive system. The characteristic length scale of this state, $\xi_F = (D\hbar/E_{\mathrm{ex}})^{1/2}$, corresponds to the pair oscillation length scale.

Since ξ_F is of the order of a few nanometers, it is necessary to use nanostructures. As the pair reservoir is separated from the ferromagnet, S/F nanostructures allow one to make a difference between phase coherence and pairing. In fact, oscillations result only from exchange field induced dephasing of the pair function in F. They are therefore less sensitive to elastic collisions and can exist even in the dirty limit. Similarly, the π-state does not require the gap and the exchange energy scales to be comparable. So the π-state is a fundamental manifestation of the FFLO state without the related constraints and is easier to realize experimentally.

The superconducting density of states induced in the ferromagnet is sensitive to interference of the pair wave function with itself (formally this comes from the fact that the density of states is given by $\mathrm{Re}(1 - FF^*)^{1/2}$, where F is the anomalous Green function [4]). Oscillations of the pair wave function in the real space manifest themselves through an interference term in the density of states. In particular, the tunneling spectrum is capsized with respect to that of the normal state at the distance from the S/F interface corresponding to the superconducting wave function sign change (see Fig. 1(a)) [5]. We measure the sign reversal of the density of states in the ferromagnet by tunneling spectroscopy using planar $S_2/F/I/S_1$ junctions with different F layer thicknesses. The ratio between dynamical conductance measured when electrode S_1 is in the normal state (G_{SN}) and when two electrodes S_1 and S_2 are in the normal state (G_{NN}) gives the superconducting density of states induced in F convolved by the Fermi function. Cross geometry junctions (inset of Fig. 1(a)) are fabricated by UHV in situ evaporation through removable mechanical masks.

The materials we have used are $S_1 = \mathrm{Al}$, $I = \mathrm{Al_2O_3}$, $F = \mathrm{Pd_{0.9}Ni_{0.1}}$ and $S_2 = \mathrm{Nb}$. We have chosen a weakly ferromagnetic alloy with a Curie temperature of the order of 100 K to diminish the exchange energy and augment ξ_F. Niobium is the natural choice because it has a high critical field and a small coherence length, making it less sensitive

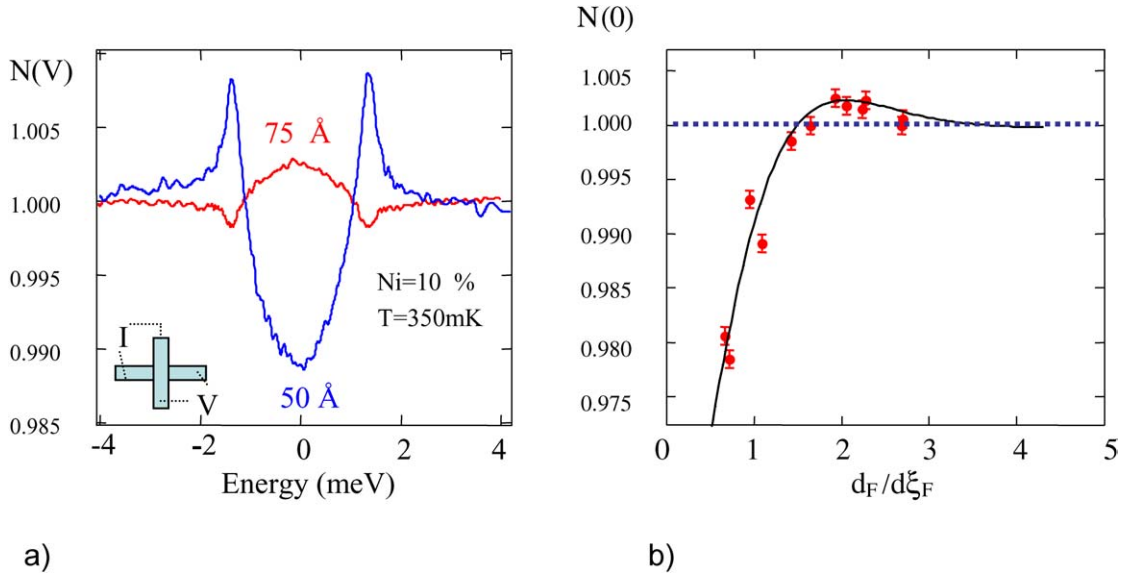

Fig. 1. Spectroscopy of the π-state [5]. (a) Density of states for two thicknesses of PdNi corresponding to a positive (50 Å) and a negative pair wave function (75 Å). The density of states is sensitive to dephasing by the ferromagnetic layer and it is capsized when the pair function is negative. Inset: cross geometry of the planar junctions. (b) Density of states at zero energy as function of the PdNi layer thickness reproduces the decaying oscillations described by Eq. (2). The full curve is best fit obtained using the formalism of the proximity effect in the diffusive material when a PdNi/Nb interface resistance of 10^{-6} Ω is taken into account [5].

to the domain structure of the ferromagnetic layer. In fact if $\xi_o \ll l_{\text{domaine}}$ (where l_{domaine} is the length of a magnetic domain), the ferromagnet can be considered as a single domain on the length scale defined by a Cooper pair. By measuring densities of states for different Ni concentrations, it is possible to determine the exchange energy, as shown below. The sign reversal of the density of states for two different PdNi thicknesses corresponding to either a positive (5 nm) or a negative (7.5 nm) pair wave function, is shown in Fig. 1(a). The density of states at zero energy as a function of the normalized PdNi layer thickness d_{PdNi}/ξ_F is shown in Fig. 1(b). It reproduces the oscillations of the pair wave function (See Eq. (2)). It is important to stress that the variations in the density of states in comparison with the normal state are of the order of one percent or less, due to the exponential decay of the pair wave function amplitude in the ferromagnet and a finite resistance of the Nb/PdNi interface that reduces the number of Cooper pairs entering the ferromagnet. The interface resistance has directly been measured in the junctions without the insulator $R_{\text{Nb/PdNi}} \approx 10^{-9}\ \Omega\,\text{cm}^2$ [6]. An additional phase shift at the interface has been recently suggested [7] and it may explain the off-set in the value of d_F introduced in the theoretical curve presented in Fig. 1(b).

Finally, it is worthwhile underlining:

(1) *Spin-orbit coupling*: if in the π-state the momentum does not need to be a good quantum number, spin, however, has to be a quantum number. If spin is not a good quantum number, the average momentum transfer to a Cooper pair is zero and the oscillations of the pair wave function disappear [4]. The spin diffusion length therefore needs to be longer than ξ_F. This imposes a limitation on the spin-orbit coupling energy: $v_F\tau_{\text{SO}} = v_F/E_{\text{SO}} > \xi_F$.

(2) *Spin injection*: the description of the superconducting proximity effect in a ferromagnet is formally identical to the description of the spin polarized transport when an out-of-equilibrium magnetization, M_{HE} is injected in a normal metal [8]. In this case, spin dephasing is due to spin precession. Eq. (2) reads:

$$M_{\text{HE}} = \int_0^\infty 1/(4\pi Dt)^{1/2} \mathrm{e}^{-x^2/4Dt} \cos(\omega_L t) \mathrm{e}^{-t/\tau_{\text{sf}}}\,\mathrm{d}t \tag{3}$$

where ω_L is the precession frequency and τ_{sf} is the spin relaxation time. Of course, the phase relation between electrons is arbitrary.

3. Spin fluctuations

A potential well whose dimension is comparable to the electron Fermi wavelength forms bound states. A similar phenomenon happens in a SNS junction, and here the potential well discontinuity is in the pair potential (or superconducting gap). Bound states in the normal metal interlayer are called Andreev bound states and their energy spectrum depends on the N interlayer thickness and the transport inside the normal metal.

Let us consider an electron in N arriving at the interface with energy E below the superconducting gap, Δ_s. At zero temperature, this electron with energy E (measured from the Fermi level) cannot penetrate the superconductor in any other way than as a part of a Cooper pair. The electron it pairs up with leaves a hole of energy $-E$ propagating with opposite momentum and spin sign (approximately, in reality the difference in momenta between the electron and the reflected hole is $2E/\hbar v_F$). The hole has the same trajectory as the electron in the opposite direction (see Fig. 2(a)). In fact, incident electron penetrates the superconductor by length of the order ξ_o before it is reflected as a hole (Andreev reflection [9]).

If we limit ourselves to diffusive transport in the normal metal, which most frequently corresponds to the experimental situation, it is better to think in terms of energy instead of momentum. The dephasing in the wave functions between an incident electron and the reflected hole is $\Delta\phi = 2Et/\hbar$. For electrons at the Fermi level, $E = 0$, superconducting correlations are in principle limited only by loss of the phase coherence.

Spectroscopy allows us to probe the Andreev bound states in the normal metal [10]. Let us first consider the S/N geometry, when two Andreev reflections take place at the same S/N interface. Bound states in the semi-infinite normal metal are related to trajectories displayed in Fig. 2(a). We stress that these states, and therefore the superconducting correlations, are formed in N because the Andreev reflection couples two trajectories that are reversed in time. At the distance $d = (Dt)^{1/2}$ from the S/N interface, $\Delta\phi = 2Ed^2/D\hbar$, the interference between an electron and a hole depends on their energies, and that gives the bound states spectrum. The inset in Fig. 2(a) shows the expected density of states. The characteristic energy $E_{\text{Th}} = \hbar D/d^2$ (Thouless energy) corresponds to $\Delta\phi = 2\pi$ [11].

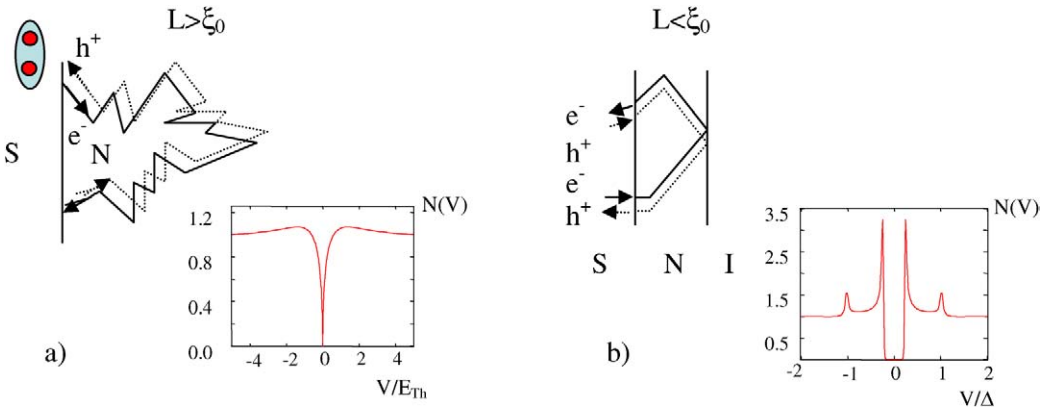

Fig. 2. Propagation of superconducting correlations in a normal metal. (a) Andreev reflection at the S/N interface: electron of the energy less than Δ_s is reflected as a hole. Bound states are formed in a semi-infinite metal corresponding to two Andreev reflections. The density of states in the normal metal is modified by these states. It shows a characteristic energy E_{Th} that depends on distance d from the S/N interface [11]. (b) In a finite size system (normal metal layer thickness is smaller than the coherence length), bound states are modified. A gap appears in the excitation spectrum, E_g, while the gap Δ_s stays visible in the density of states, but with a reduced spectral weight [12].

Let us now consider finite size effects. If the metal thickness is $d_N < \xi_o$ (i.e., $E_{Th} > \Delta_s$), the interference between an electron and a hole will be given by trajectories represented in Fig. 2(b). In particular, the diffusion time has to be replaced by the time an electron spends in N, $\tau_N \sim d_N/v_F$, that becomes comparable to the time it spends in S. Constructive interference between the electron and the hole ($\Delta\phi = 2\pi$) can take place only for energies higher than $E_g = \pi\sigma\hbar/\tau_N$, which is of the same order as the superconducting gap (σ is the transparency). E_g defines a mini-gap in the N excitation spectrum [12]. It is called the induced gap and it also depends on the S/N interfacial transparency, or, in the other words, on the length of the trajectory of an electron in the normal metal before it undergoes to an Andreev reflection. The density of states for a system of finite size is shown in the inset in Fig. 3(b). Two characteristic energies appear: the induced gap E_g and the superconducting gap Δ_s.

Bound states in the normal metal are sensitive to interactions. We can therefore use the proximity effect as a probe of electron correlations. Specifically, in a paramagnetic metal, the exchange between electrons increases approaching the ferromagnetic transition and gives rise to spin fluctuations (paramagnons [13]). If the fluctuation energy is bigger than the superconducting gap, the effect on the electrons with energy $E < \Delta_s$ is to renormalize the energy E which becomes $E(1 + \lambda_p)$ [14], where λ_p is the electron-spin fluctuation coupling constant. The gap induced in the normal metal is reduced as $E_{gs} = E_g/(1 + \lambda_p)$. Measurement of the induced gap by tunneling spectroscopy gives directly the coupling constant λ_p [15].

Recent developments in the theory of the superconducting proximity effect in the diffusive limit allow a quantitative analysis of the density of states in the normal metal [16,17]. In particular, the effect of electron energy renormalization by the spin fluctuations is easily incorporated in the Usadel formalism [18]:

$$\frac{\hbar D_N}{2}\frac{\partial\theta}{\partial x^2} + \mathrm{i}(1+\lambda_{sf})E\sin\theta + \Delta_N\cos\theta = 0 \tag{4}$$

where D_N, Δ_N and λ_N are, respectively, the diffusion constant, the gap and the effective electron-electron coupling in the normal metal. The Pairing angle θ that is related to the Green functions by angular parametrization, also contains information on equilibrium properties and in particular the density of states as function of the distance from the S/N interface, $N(E, x) = \mathrm{Re}(\cos\theta)$.

The superconducting density of states induced in the thin layers of Ag, Pt, Pd and PdNi of the same thickness of 5 nm is given in Fig. 3(a), as well as the theoretical curves obtained self-consistently from the Usadel equation (4) [18]. The junction geometry is the same as that described above. The Nb mean free path is 90 Å, its critical temperature 8.5–8.7 K and coherence length is 80 Å. In the paramagnetic regime, the electron-spin fluctuations coupling constant increases when approaching the ferromagnetic instability while the induced gap diminishes as can be seen in Fig. 3(a). From the fits one gets λ_p to be 0.05, 2.05, 4.15, 5.3 for Ag, Pt, Pd and $Pd_{0.99}Ni_{0.01}$, respectively (here the density of Ni impurities in Pd is less than 2.4% and the alloy is paramagnetic). The Stoner factor S is 1, 3.3, 10 and 18 for Ag, Pt, Pd and $Pd_{0.99}Ni_{0.01}$, respectively. The Stoner factor diverges when approaching the paramagnetic/ferromagnetic

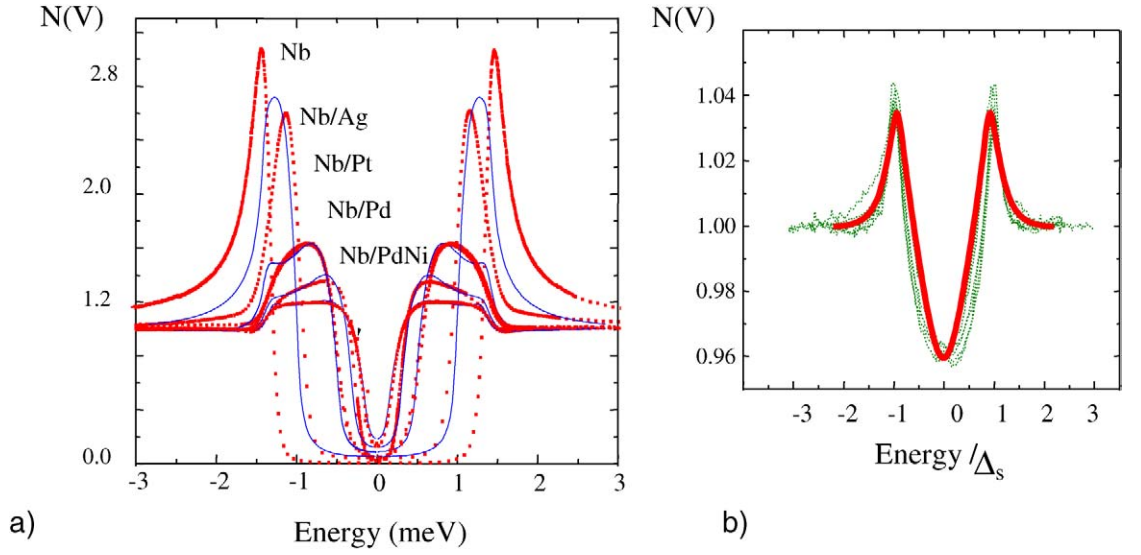

Fig. 3. Superconducting proximity effect approaching the paramagnetic-ferromagnetic transition [15]. (a) Superconducting density of states induced in Ag, Pt, Pd and PdNi as function of the voltage across the junction. In the paramagnetic state interactions electron-paramagnon reduce the induced gap E_g. Proximity-Effect-Tunneling Spectroscopy (PETS) [16] gives the constant of electron-paramagnon coupling and the Stoner factor. (Best fits obtained as self-consistent resolution of the Usadel equations are presented as blue curves). (For interpretation of the references to colour, the reader is referred to the web version of this article.) (b) Density of states in the ferromagnetic state for PdNi layers (Ni concentration is between 5.5 and 12%). The curve $N(V)$ presents only one characteristic energy: Δ_s. Strong pair-breaking in F destroys finite size effects and the induced gap disappears. Curves are normalized by an amplitude factor directly related to the exchange energy (see Eq. (6)). The theoretical calculation is presented in the red line. The paramagnetic and ferromagnetic layer thickness is 50 Å.

transition. When we increase the concentration of Ni in Pd, the magnetically polarized area around every Ni impurity (neutron diffraction measurements give $\xi_{pl} \approx 1.5$ nm) [19] becomes of the same size as the distance between the impurities and the system becomes ferromagnetic.

In the ferromagnetic state, the pair breaking by the exchange energy is so strong that the system loses the finite size effects because $d > \xi_F$. This is seen as a modification of the continuum of bound states and more precisely by the disappearance of the induced gap. The density of states shows only one characteristic energy, the niobium gap energy. Like the spin fluctuation effects, the exchange energy is naturally incorporated in the Usadel equations [4]:

$$\frac{\hbar D_N}{2}\frac{\partial \theta_\sigma}{\partial x^2} + \mathrm{i}(E + \sigma E_{ex})\sin\theta_\sigma = 0 \tag{5}$$

where $\sigma = \pm 1$ is the electron spin orientation. The total density of states is given by $N(E,x) = \mathrm{Re}\{\cos\theta_+ + \cos\theta_-\}/2$. Linearization for small values of θ gives the density of states in the ferromagnet

$$N(E,x) = 1 + \big[N_o(E) - 1\big]\exp\big(-2\sqrt{E_{ex}/E_{th}}\big)\cos\big(2\sqrt{E_{ex}/E_{th}}\big) \tag{6}$$

where N_o is the density of states at the S/F interface and E_{Th} is the Thouless energy.

This expression illustrates the sign change of the density of states described above. In fact, the phase term E_{ex}/E_{Th} (equivalent to $\Delta\phi = \Delta p.x$ in (1) in the dirty limit) modulates the amplitude and sign of the density of states, while the energy dependence is factorized. In general, unlike in a normal metal, the superconducting proximity effect in a ferromagnet is very short range (10–100 Å) as the Thouless energy must be comparable to the exchange energy and not to the thermal energy.

Fig. 3(b) shows the density of states measured for 50 Å Pd_1Ni_{1-x} layer thickness for different Ni concentrations ($5.5 < x < 12\%$ Ni) and therefore different exchange energies. Densities of states, normalized by the amplitude factor $e^{-2(E_{ex}/E_{Th})^{1/2}}\cos(2(E_{ex}/E_{Th})^{1/2})$ (or in an equivalent way $e^{-2d/\xi_F}\cos(2d/\xi_F)$, are independent of the exchange energy as Eq. (6) indicates. Eq. (6) is represented in Fig. 4(b) by a thick curve. We obtain the exchange energy from the amplitude factor and the Thouless energy, which depends only on the magnetic layer thickness ($d = 50$ Å) and the diffusion constant. E_{ex} is 0.1, 0.5, 2.8, 3.3 and 3.9 for a Ni concentration of 5.5, 6.0, 7.0, 9.8, 11.5%, respectively [15].

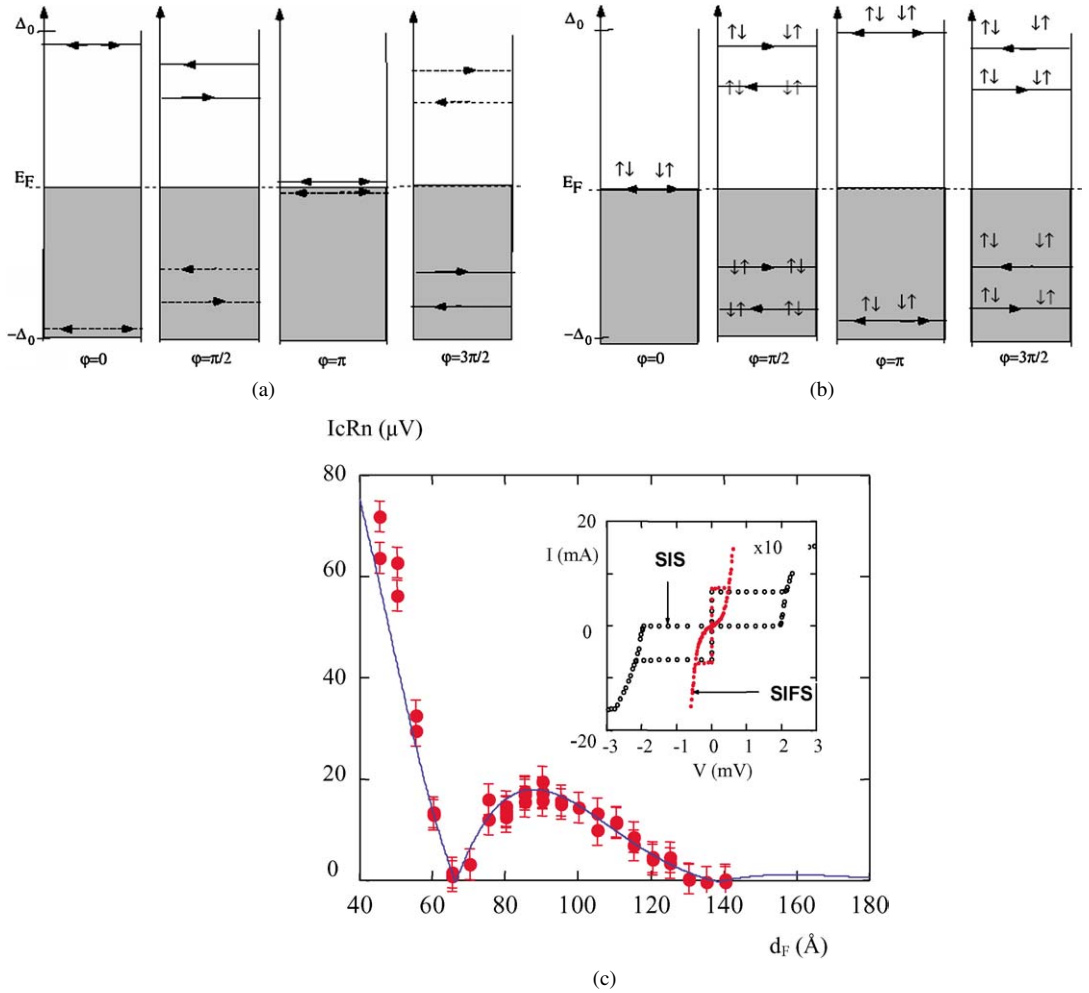

Fig. 4. Oscillations of the critical current of the SIFS junction [21]. (a) Dependence of the Andreev bound states of a short SNS Josephson junction on the phase difference between two superconductors [6]. (b) π-SFS junction. The bound state is at zero energy for a zero phase difference. Arrows define the direction of the current flow. (c) Josephson coupling as a function of the PdNi layer thickness. The critical current reaches zero for approximately 6.5 nm. This is the critical thickness corresponding to the crossover between the 0 and the π-state of the junction. The full line is the best fit from the theory. Insert: current-voltage characteristic of a junction without (black curve) and with (red curve) a ferromagnetic PdNi layer (Ni 12%).

4. Ferromagnetic-π junctions

For a SNS junction, the Andreev bound states can transmit a non-dissipative current between the two superconductors. This is the Josephson effect [20] and it consists of a transfer of Cooper pairs between two superconducting electrodes. Since the bound states energy depends on the phase difference between the two electrodes, $\Delta\varphi_{12}$, the current across the junction depends on $\Delta\varphi_{12}$. Non-dissipative current density of every bound state depends on its energy. It defines the maximum coherent current that every bound state can transport.

Andreev levels for a short SNS Josephson junction ($\Delta_s < E_{Th}$, or equivalently $\xi_o > L$) for different phase differences between two superconductors are represented in Fig. 4(a) [6]. Arrows note the current flow direction: positive current corresponds to an electron going from right to left and vice versa. For a short junction, in the ballistic limit, there is only one bound state between the Fermi level and the superconducting gap. We note that for $\Delta\varphi_{12} = 0$ and π, the bound state is doubly degenerate, equal amounts of positive and negative current are transmitted and total current is zero. For $\Delta\varphi_{12} = \pi/2$, total current is positive because the bound states closer to the gap transmit more current. For $\Delta\varphi_{12} = 3\pi/2$, the current is negative. Andreev levels for a short SFS junction with $E_{ex} \approx E_{Th}$ are represented

in Fig. 4(b). We note that the same bound states are obtained for a phase shift of π between two superconducting electrodes. This shift is due to the exchange energy dependent phase factor given to an electron or a hole after the Andreev reflection. This type of Josephson junction is called a π junction. If the transport in the ferromagnetic layer is diffusive, we obtain a continuous spectrum of bound states. Then we consider the spectral density of current, i.e., non-dissipative current distributed by the bound states continuum as function of energy. Spectral current density for an SFS junction changes sign for $x \approx \xi_F$ ($E_{\mathrm{ex}} \approx E_{\mathrm{Th}}$), where x is the thickness of the ferromagnetic layer [21].

We can take into account this sign change of the Josephson current by a simple argument. If we couple the superconducting wave function induced in F by proximity effect (S/F) with the other superconducting electrode, if this coupling is sufficiently weak (we take only the first harmonic in the current phase relation), and the Josephson energy in the first order is: $E_J = -\mathrm{Re}(\Psi_F \Psi_{S2}^*)$ then, by using Eq. (2), we obtain the Josephson current: $J = -\partial E/\partial(\Delta\varphi_{12}) = J_{\mathrm{o}} \cos(x/\xi_F)\mathrm{e}^{-x/\xi_F} \sin(\Delta\varphi_{12}) = J_{\mathrm{c}} \sin(\Delta\varphi_{12})$. This relation gives the value of non-dissipative current across the Josephson junction as function of the phase difference between two superconductors. The product $J_{\mathrm{o}} \cos(x/\xi_F)\mathrm{e}^{-x/\xi_F}$ defines the critical current of the junction. It reproduces the exponential decay of the superconducting wave function in F. The sign change in the critical current corresponds to a π phase shift in the current phase relation.

The critical current of a Josephson junction is measured from the I–V characteristic. It corresponds to the switching current in the dissipative branch. The I–V characteristics are obtained by current bias. The I–V characteristic of an SFIS junction is shown in the inset of Fig. 4(c). Here the insulating layer has the role of considerably reducing the junction conductance.

For high values of the McCumber parameter, $\beta_{\mathrm{c}} = 2\mathrm{e}I_{\mathrm{c}}/\hbar\ R_N^2 C$ the I–V characteristic is hysteretic (C is the junction capacitance). As previously described, junctions are fabricated in situ with removable mechanical masks. The bottom electrode is made up of 150 nm of Nb covered with 50 nm of Al oxidized by an oxygen plasma ($P = 8 \times 10^{-2}$ mbar). The ferromagnetic Ni concentration of the PdNi ferromagnetic layer is 12–14% of Ni. The upper electrode is 500 Å of Nb. The Josephson coupling, i.e., the critical current multiplied by the junction resistance in the normal state ($V \gg \Delta_{\mathrm{s}}$), as function of the ferromagnetic layer thickness is given in Fig. 4(c). It reproduces the oscillations of the superconducting wave function in F. Similar experiments performed using a CuNi alloy instead of PdNi show the same results [22]. However, by measuring the I–V characteristic, one only addresses the absolute value of the Josephson coupling, as it is impossible to control simultaneously the phase difference and the current across the junction. The full curve corresponds to a theoretical calculation. A finite Nb/PdNi interface resistance $\approx 10^{-9}\ \Omega\,\mathrm{cm}^2$ is introduced.

5. π-SQUID

One can measure a phase difference with an interferometer. Let us consider a superconducting ring interrupted by two Josephson junctions [23] (a dc-SQUID). The superconducting current in the SQUID is given by the sum of Josephson currents of the two junctions: $I = I_{\mathrm{c}1} \sin\varphi_1 + I_{\mathrm{c}2} \sin\varphi_2$, where φ_1 and φ_2 are phase differences across the junctions 1 and 2. The effective flux Φ in the ring is the sum of the applied flux Φ_{ex} and the screening flux created by the ring itself, LI_{s}: $\Phi = \Phi_{\mathrm{ext}} - LI_{\mathrm{s}}$, where L is the inductance of the ring and I_{s} is the induced current. The phase relation across the ring is $\varphi_2 - \varphi_1 = 2\pi\Phi/\Phi_{\mathrm{o}} + 2n\pi + \delta_1 + \delta_2$, where δ_1 and δ_2 are intrinsic phase differences across the two junctions. We get the critical current of the dc-SQUID by maximizing the total current (i.e., for $\mathrm{d}I/\mathrm{d}\varphi_1 = 0$). When the critical currents of the two junctions are identical, $I_{\mathrm{c}1} = I_{\mathrm{c}2} = I_{\mathrm{co}}$, we find:

$$I_{\mathrm{c}} = I_{\mathrm{co}} \cos\bigl(\pi\Phi/\Phi_{\mathrm{o}} + (\delta_1 + \delta_2)/2\bigr) \tag{7}$$

The critical current of the ring depends on the flux [24] and on the intrinsic phase difference of each junction. Note that if one junction of the dc-SQUID is in the 0-state and the other in the π-state (π-SQUID), the critical current at zero flux is zero because currents in the two arms of the SQUID circulate in opposite directions. In that way, the interference pattern of a π-SQUID presents a half flux quantum shift [25]. This corresponds to the π phase shift produced by the π junction.

We have developed suspended masks for angle evaporation and lift off of Nb. These masks are produced by electron lithography. A SEM (Scanning Electron Microscope) picture of the mask before evaporation is presented in Fig. 5(a). A 50 nm thick Ge layer is deposited on a PES resist (Phenylene-Ether-Sulphone) that has a vitreous transition at

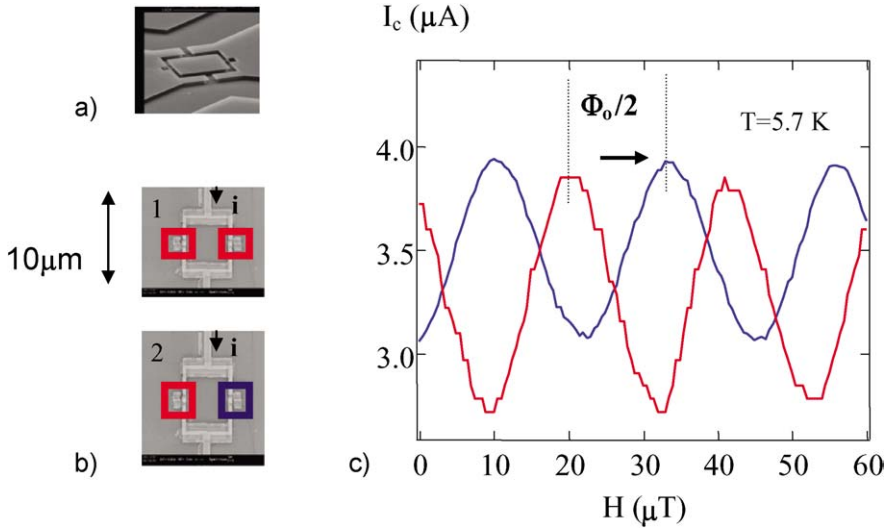

Fig. 5. Measurement of the ground state of a π junction by an interferometer technique [26]. (a) SEM picture of a suspended mask prepared by electron lithography to define the SQUID geometry. (b) SEM image of two SQUIDs after evaporation and lift off of the resist mask (PES). A ferromagnetic junction is inserted in both arms of the SQUIDs. SQUID 1 is formed by two 0 junctions (0-SQUID) indicated by red squares. SQUID 2 is formed by a 0 junction and a π junction (π-SQUID) indicated by a blue square. (c) Critical current, I_c, as function of the applied magnetic field. The π-SQUID displays a shift by a half flux quantum in the I_c corresponding to the π phase shift produced by the π junction.

235 °C. The mask and the resist are lifted off after evaporation. The SQUIDs, whose size is approximately 8 μm, consist of a Nb ring interrupted by two Josephson junctions Nb/NbO/$Pd_{0.88}Ni_{0.12}$/Nb. SEM pictures of two SQUIDs with a 0 and a π junction (π-SQUID), and two 0 junctions (0-SQUID), are shown in Fig. 5(b) (red squares denote 0 junctions and a blue square denotes a π junction). Zero and π junctions correspond to two different $Pd_{0.88}Ni_{0.12}$ layer thicknesses. Ferromagnetic junctions are obtained by angle evaporation. The Nb layer is oxidized at $P = 1$ mBar for 3–5 minutes in order to reduce the junction critical current. Thus we obtain normal state resistance of the order of tenths of ohms for a surface 0.8 μm × 1 μm and critical current values of 10 μA at 5 K. The ring inductance is around 30 pH, SQUID screening is weak $I_c L \approx 0.1\Phi_o$ at that temperature and the SQUID is in the linear limit.

In Fig. 5(c) we present variations of the critical current as function of the magnetic flux for the 0-SQUID and the π-SQUID shown in Fig. 5(b). We observe a shift by a half flux quantum in the interference patterns as expected [26]. We note that the amplitude of oscillations of the critical current is much less than that expected from theory. Asymmetrical junctions and non-sinusoidal current-phase relation can explain this reduction in amplitude [27]. A π junction can be used as phase generator for macroscopic quantum experiments.

6. Spontaneous macroscopic current

Let us consider a superconducting ring interrupted by a π junction. The free energy of this device is given by adding the magnetic energy of the ring with the Josephson energy of the junction. It can be written as:

$$F = LI^2/2 - \mathrm{abs}(E_J)\Phi_o/2\pi \cos(2\pi\Phi/\Phi_o + \pi) \tag{8}$$

We present in Fig. 6(a) the free energy F as function of the magnetic flux in the ring for zero applied magnetic field and different values of the parameter $\gamma = I_c L/\pi\Phi_o$. In the linear limit $|\gamma| \ll 1$ the magnetic energy dominates the response of the ring and the energy minimum corresponds to zero magnetic flux in the ring. On the other hand, in the non-linear limit $|\gamma| \gg 1$, the Josephson energy dominates and the free energy is a double-well potential. In the ground state a spontaneous flux is generated in the ring [28]. This flux is produced by a spontaneous supercurrent that compensates the π phase produced by the ferromagnetic junction. The ground state is twice degenerated because two energy minima are identical and symmetric flux-wise. They correspond to a flux entering or leaving the plane of the ring and current circulating respectively clockwise or anti-clockwise.

The detection of the half flux quantum in an isolated superconducting/ferromagnetic ring can be realized with a magnetometric probe directly coupled to the ring. We have deposited by suspended mask technique described above

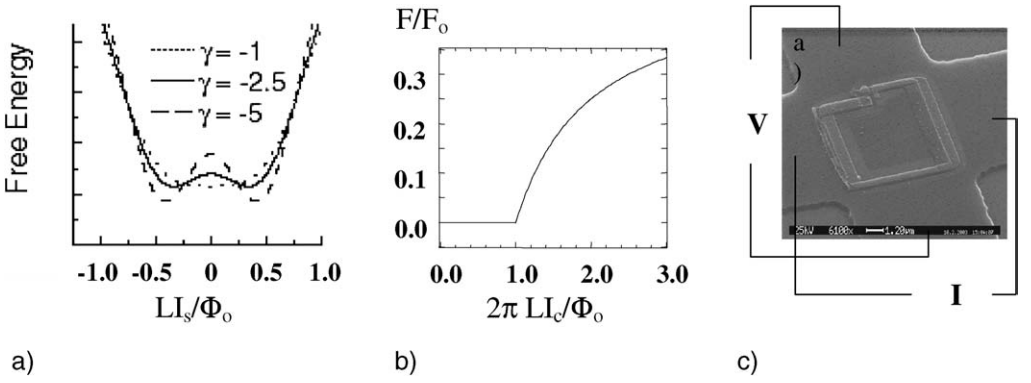

Fig. 6. Spontaneous current of the superconducting ring interrupted by a ferromagnetic π junction [29]. (a) Free energy of the ring as function of the flux in the ring for different values of the parameter gamma (see text). (b) Phase transition as function of the product $I_c L$ in the ring. If $I_c L \gg \Phi_o$ (non-linear limit), the phase difference produced by the PdNi π junction is compensated by the spontaneous supercurrent that generates a half flux quantum in the ring. (c) SEM picture of the experimental setup used to measure the spontaneous flux. The S/F ring is placed on the Hall probe obtained by electron lithography. The field associated with the spontaneous magnetic flux produces a Hall signal. Contact setup for current (I) and voltage (V) on the Hall probe.

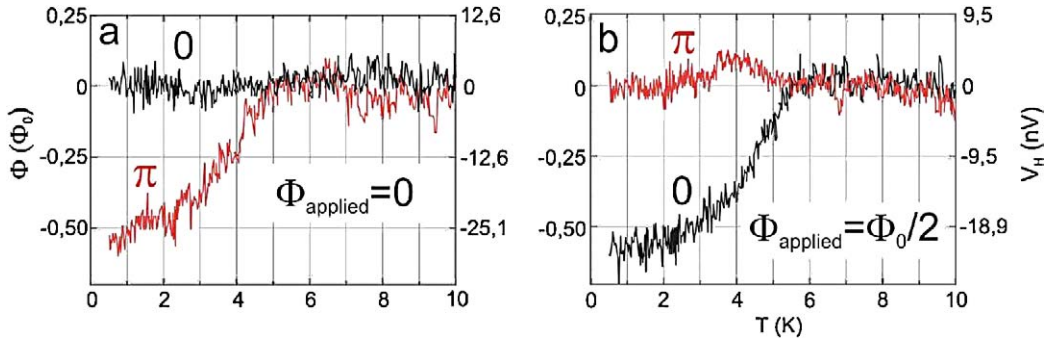

Fig. 7. Measurement of the spontaneous flux in a S/F ring [29]. (a) Diamagnetic signal appears in the π ring below the critical temperature of the superconductor (Nb). At low temperature, this signal is equal to a half flux quantum in the ring. No signal is detected for the ring with a 0 junction. (b) Field-cool measurements show that the spontaneous flux in the π-SQUID is cancelled by the screening current. The response of the 0 ring is identical to the response of the π-SQUID in the zero cool field.

a superconducting ring of Nb (80 nm thick) interrupted by a PdNi junction of thickness 7.5 nm corresponding to π-coupling over a Hall cross fabricated from 2DEG. (To have a control measurement, we have also prepared a ring with a 0 junction.) We have chosen a PdNi thickness corresponding to maximum π-coupling (the Ni concentration is 18–20%) in order to minimize the effects of thickness fluctuations. The Hall sensor measures the magnetic field produced by the spontaneous current in the ring, the Hall voltage being directly proportional to the magnetic field. An SEM picture of the device consisting of the ring and the Hall cross is shown in Fig. 6(c). The size of the Hall cross is 8 μm × 8 μm, and the size of the ring is 6 μm × 6 μm.

The phase transition as function of the parameter $I_c L$ is second order. The flux in the ring as function $I_c L$ is shown in Fig. 6(b). The critical point is given by $2\pi I_c L = \Phi_o$. For rings with $I_c L \gg \Phi_o$, the spontaneous flux inside the ring is equal to a half flux quantum.

In Fig. 7(a) we present the Hall signal measured as function of temperature for a π ring and a 0 ring, interrupted respectively with one π and one 0 junction. As expected, the Hall signal is detected below the Nb critical temperature only for a π ring [29,30]; as a function of temperature it follows the critical current of the junction [29]. In Fig. 7(b) is shown the Hall signal as function of temperature in the presence of the magnetic field (field-cool) corresponding to a half flux quantum in the ring for the same rings as Fig. 7(a). The behaviour is inverted: no Hall signal is detected for a π ring while a signal appears for a 0 ring. Spontaneous current generated by the π junction is totally compensated by the screening current. This allows us to calibrate the spontaneous flux as equal to the compensation flux, i.e., one half flux quantum. Hall signals in zero-field-cool for a π ring and field-cool for a 0 ring are comparable. Indeed, the

screening current trapped in the ring on a field cool corresponding to half flux quantum in the ring is identical to that produced by a π junction.

7. Conclusions

We have presented a series of experiments in which the interplay between ferromagnetic order and superconductivity gives rise to new ground states. S/F nanostructures are unique in the sense that they do not require comparable energy scales (i.e., an exchange energy of the order of the superconducting gap).

Specifically, tunneling spectroscopy at the paramagnetic-ferromagnetic transition allows one to address the enhanced exchange interaction between quasiparticles. By fitting the density of states, the Stoner factor is measured in the paramagnetic regime, while the exchange energy is obtained in the ferromagnetic regime. Furthermore, a new inhomogeneous superconducting state ("π"-superconductivity) is induced into F. This state is revealed by oscillations of the induced superconducting density of states in F and it is the equivalent of the FFLO state predicted in bulk superconductor. The proximity induced FFLO state is more robust that the bulk FFLO with respect to disorder and exchange field, but it vanishes, in the dirty limit, on about 100 Åfrom the interface.

"π"-superconductivity produces "π"-coupling when ferromagnetic Josephson junction is formed by coupling the ferromagnetic layer with a second superconductor ("π"-junction). The "π"-coupling has been measured by Josephson interferometry and it corresponds to a π-phase shift in the current-phase relationship of the junction. Thus, "π"-coupling can be used as a 'phase-battery' for macroscopic quantum effects. In particular, we have observed a spontaneous half quantum flux in a superconducting ring with a "π"-junction. The ground state is degenerated and corresponds to either a vortex or an antivortex with equal probability [30].

Acknowledgements

It is unfortunately impossible to acknowledge all the colleagues that helped us with comments and suggestions. We apologize for that. However, we want to address some special thanks. M.A, T.K and M.L.D.R. are indebted to L. Dumoulin, H. Pothier and D. Esteve for many fruitful discussions. W.G. and P.G. acknowledge T. Fournier for technical assistance. A.B. and C.S. thank M. Reinwald and W. Wegscheider for the 2DEG Hall probes. Finally M.A. is indebted to I. Petkovic for a critical reading of the manuscript.

References

[1] A.M. Clogston, Phys. Rev. Lett. 9 (1962) 266.
[2] P. Fulde, R.A. Ferrell, Phys. Rev. 135 (1964) A550.
[3] A.I. Larkin, Yu.N. Ovchinnikov, Sov. Phys. JETP 20 (1965) 762.
[4] A. Buzdin, Rev. Mod. Phys. 77 (2005) 935.
Z. Radović, M. Ledvij, L. Dobrosavljević-Grujić, A.I. Buzdin, J.R. Clem, Phys. Rev. B 44 (1991) 759–764.
See also E.A. Demler, G.B. Arnold, M.R. Beasley, Phys. Rev. B 55 (1997) 15174.
[5] T. Kontos, M. Aprili, J. Lesueur, et al., Phys. Rev. Lett. 86 (2001) 304.
[6] W. Guichard, Thèse (Université Joseph Fourier, Grenoble, 2003).
[7] A. Cottet, W. Belzig, Phys. Rev. B R72 (2005) 180503.
[8] F.J. Jedema, et al., Nature 416 (2002) 713.
[9] A.F. Andreev, Sov. Phys. J. Exp. Theor. Phys. 19 (1964) 1228.
[10] P.G. De Gennes, D. Saint-James, Phys. Lett. 4 (1963) 151.
[11] S. Guéron, H. Pothier, N.O. Birge, D. Esteve, M.H. Devoret, Phys. Rev. Lett. 77 (1996) 3025–3028.
[12] W.L. McMillan, Phys. Rev. 175 (1968) 573.
[13] D.L. Mills, P. Lederer, J. Phys. Chem. Solids 27 (1966) 1805.
[14] J.M. Daams, B. Mitrovic, J.P. Carbotte, Phys. Rev. Lett. 46 (1981) 65–68.
[15] T. Kontos, M. Aprili, J. Lesueur, X. Grison, L. Dumoulin, Phys. Rev. Lett. 93 (2004) 137001.
[16] E.L. Wolf, Principles of Electron Tunneling Spectroscopy, Oxford Univ. Press, New York, 1985.
[17] A.A. Golubov, et al., Phys. Rev. B 51 (1995) 1073.
[18] J.W. Serene, D. Rainer, Phys. Rep. 101 (1983) 221.
[19] A.T. Alfred, B.D. Rainford, M.W. Stringfellow, Phys. Rev. Lett. 24 (1970) 897.
[20] B.D. Josephson, Phys. Rev. Lett. 1 (1962) 251.
[21] T. Kontos, M. Aprili, J. Lesueur, F. Genêt, B. Stephanidis, R. Boursier, Phys. Rev. Lett. 89 (2002) 137007-1.
[22] V.V. Ryazanov, V.A. Oboznov, A.V. Veretennikov, A.Y. Rusanov, Phys. Rev. B 65 (2002) 020501.

[23] S.T. Ruggiero, D.A. Rudman (Eds.), Superconducting Devices, Academic Press, San Diego, 1990.
[24] A. Barone, G. Paterno, Physics and Applications of the Josephson Effect, John Wiley and Sons, New York, 1982.
[25] D.A. Wollman, D.J. Van Harlingen, A.J. Leggett, Phys. Rev. Lett. 73 (1994) 1872.
[26] W. Guichard, M. Aprili, O. Bourgeois, T. Kontos, J. Lesueur, P. Gandit, Phys. Rev. Lett. 90 (2003) 167001-1.
[27] K. Hasselbach, D. Mailly, J.R. Kirtley, J. Appl. Phys. 91 (2002) 4432.
[28] L.N. Bulaevskii, V.V. Kuzii, A.A. Sobyanin, Solide State Comm. 25 (1978) 1053.
See also C.C. Tsuei, J.R. Kirtley, Rev. Mod. Phys. 72 (2000) 969–1016.
[29] A. Bauer, J. Bentner, M. Aprili, M.L. Della Rocca, M. Reinwald, W. Wegscheider, C. Strunk, Phys. Rev. Lett. 92 (2004) 217001.
[30] M.L. Della Rocca, M. Aprili, T. Kontos, A. Gomez, P. Spathis, Phys. Rev. Lett. 94 (2005) 197003.